

Title:

Active subthreshold dendritic conductances shape the local field potential

Abbreviated title:

Active dendritic conductances shape the LFP

Author names and affiliation:

Torbjørn V Ness, Department of Mathematical Sciences and Technology, Norwegian University of Life Sciences, 1432 Ås, Norway.

Michiel W H Remme, Institute for Theoretical Biology, Humboldt University Berlin, 10115 Berlin, Germany.

Gaute T Einevoll, Department of Mathematical Sciences and Technology, Norwegian University of Life Sciences, 1432 Ås, Norway; Department of Physics, University of Oslo, 0316 Oslo, Norway.

Corresponding author:

Gaute T Einevoll, Department of Mathematical Sciences and Technology, Norwegian University of Life Sciences, 1432 Ås, Norway; gaute.einevoll@nmbu.no

Active subthreshold dendritic conductances shape the local field potential

Torbjørn V Ness¹, Michiel W H Remme², and Gaute T Einevoll^{1, 3*}

¹Department of Mathematical Sciences, Norwegian University of Life Sciences, Ås, Norway

²Institute for Theoretical Biology, Humboldt University Berlin, Berlin, Germany

³Department of Physics, University of Oslo, Oslo, Norway

Key points summary

- The local field potential (LFP), the low frequency part of extracellular potentials recorded in neural tissue, is often used for probing neural circuit activity. Interpreting the LFP signal is difficult, however.
- While the cortical LFP is thought to mainly reflect synaptic inputs onto pyramidal neurons, little is known about the role of the various subthreshold active conductances in shaping the LFP.
- By means of biophysical modeling we obtain a comprehensive qualitative understanding of how the LFP generated by a single pyramidal neuron depends on type and spatial distribution of active subthreshold currents.
- For pyramidal neurons, the h-type channels likely play a key role and can cause a distinct resonance in the LFP power spectrum.
- Our results show that the LFP signal can give information about the active properties of neurons and imply that preferred frequencies in the LFP can result from those cellular properties instead of, e.g., network dynamics.

*Corresponding author: gaute.einevoll@nmbu.no

Abstract

The main contribution to the local field potential (LFP) is thought to stem from synaptic input to neurons and the ensuing subthreshold dendritic processing. The role of active dendritic conductances in shaping the LFP has received little attention, even though such ion channels are known to affect the subthreshold neuron dynamics. Here we used a modeling approach to investigate the effects of subthreshold dendritic conductances on the LFP. Using a biophysically detailed, experimentally constrained model of a cortical pyramidal neuron, we identified conditions under which subthreshold active conductances are a major factor in shaping the LFP. We found that particularly the hyperpolarization-activated inward current, I_h , can have a sizable effect and cause a resonance in the LFP power spectral density. To get a general, qualitative understanding of how any subthreshold active dendritic conductance and its cellular distribution can affect the LFP, we next performed a systematic study with a simplified model. We found that the effect on the LFP is most pronounced when (1) the synaptic drive to the cell is asymmetrically distributed (i.e., either basal or apical), (2) the active conductances are distributed non-uniformly with the highest channel densities near the synaptic input, and (3) when the LFP is measured at the opposite pole of the cell relative to the synaptic input. In summary, we show that subthreshold active conductances can be strongly reflected in LFP signals, opening up the possibility that the LFP can be used to characterize the properties and cellular distributions of active conductances.

Abbreviations list

LFP, Local Field Potential; PSD, Power Spectral Density

Introduction

The local field potential (LFP), the low-frequency part ($\lesssim 500$ Hz) of the extracellular potential recorded in the brain, has experienced a rejuvenated interest in the last decade. This is partly due to the development of novel silicon-based microelectrodes with tens or hundreds of electrode contacts covering large volumes of brain tissue, the realization that the LFP offers a unique window into neural population activity, and the possibilities offered by the signal in steering neuroprosthetic devices (Buzsáki et al., 2012; Einevoll et al., 2013a). The interpretation of the LFP signal in terms of neural activity is challenging, however, as in general thousands of neurons contribute to the recorded signal (Lindén et al., 2011). Careful mathematical modeling is thus needed to take full advantage of the opportunities that the LFP signal offers (Einevoll et al., 2013a).

Fortunately, the biophysical origin of the LFP signals seems well understood in the context of volume conduction theory (Nunez and Srinivasan, 2006), and a forward-modeling scheme linking transmembrane neural currents to recorded electrical potentials, including LFPs, has

been established (Rall and Shepherd, 1968; Holt and Koch, 1999). The forward-modeling scheme has been successfully used to study the cortical LFP signal generated by single neurons (Lindén et al., 2010) as well as cell populations (Pettersen et al., 2008; Lindén et al., 2011; Łęski et al., 2013; Tomsett et al., 2015). These studies showed, for example, that the lower frequencies of the synaptic input current give the largest contributions to the LFP for two reasons. First, the lowest frequencies give the largest transmembrane current dipole moments due to the filtering properties of dendrites (Lindén et al., 2010). Second, increased correlations in synaptic input to a population of neurons can strongly amplify the LFP signal (Lindén et al., 2011; Einevoll et al., 2013a,b), and this amplification is strongest for the lowest input frequencies (Łęski et al., 2013). Further, the amplification of the LFP due to synaptic input correlations requires the input to be asymmetrically distributed over the dendrites (Lindén et al., 2011; Łęski et al., 2013).

However, these studies were typically carried out using neuron models with passive dendrites. Neurons express a variety of active conductances that are distributed in specific ways across both soma and dendrites (Stuart et al., 2007). For example, the h-type current is most densely concentrated in the distal apical dendrites (Williams and Stuart, 2000; Magee, 1998), whereas the M-type slow potassium current is mostly localized close to the soma (Hu et al., 2007). It is well established that such active conductances affect the subthreshold processing of synaptic input (see, e.g., Remme and Rinzel 2011; Major et al. 2013). This is highly relevant for understanding the LFP signal, since, in cortex, the LFP is thought to mainly reflect synaptic currents and their associated return currents (Mitzdorf, 1985; Einevoll et al., 2007, 2013a).

Here we use a modeling approach to investigate specifically the role of voltage-dependent conductances in shaping the LFP in the subthreshold regime. We focused on pyramidal cells since they are thought to be the main contributor to the LFP in cortical recordings (Einevoll et al., 2013a) and used the state-of-the-art cortical layer 5 pyramidal neuron model by Hay et al. (2011) as a starting point for our investigation. With this highly detailed model we established that subthreshold active conductances can indeed have a sizable impact on the LFP signal. Using a simplified neuron model that used generalized descriptions of active conductances, so-called quasi-active currents (Koch, 1984; Remme, 2014), we were able to obtain an understanding of how any active conductance can affect the LFP, depending on the characteristics of the current and its distribution across the neuron.

Methods

Pyramidal neuron model

Numerical simulations for Figures 1 and 2 were carried out using a model of a cortical layer 5 pyramidal cell that was published by Hay et al. (2011). This model has a detailed morphology

and includes ten active ionic conductances fitted to experimental data by multi-objective optimization with an evolutionary algorithm. For simulations of a passive model, the active conductances were removed from the model. Simulations with a so-called "frozen" h-type conductance were performed by keeping the gating variable of the h-current constant, yielding an additional passive conductance. The original model showed a voltage gradient from soma to distal apical dendrites. In order to simplify the interpretation of the simulation results, we adjusted the leak reversal potential of each compartment such that we could set the resting potential uniformly to a specified chosen potential (Carnevale and Hines, 2006).

The neuron model received either excitatory synaptic input or white-noise current input. Synaptic inputs were modeled as steps in the synaptic conductance followed by an exponential decay with a time constant of 2 ms and used a reversal potential of 0 mV. The white-noise current input consisted of a sum of sinusoids with identical amplitudes but random phases for each integer frequency from 1 Hz to 500 Hz (see Lindén et al. 2010). The resulting white-noise signal was scaled to obtain current fluctuations with a standard deviation of 8 pA. Injection of this input into the distal apical dendrite at a distance of 1094 μm away from the soma of the active cell held at -60 mV yielded local membrane potential fluctuations with a standard deviation of 1.5 mV. The exact same white-noise input was used in all simulations (i.e., so-called "frozen" noise).

Quasi-active approximation of voltage-dependent ion currents

Voltage-dependent membrane currents often behave in a near-linear fashion for small perturbations around a holding potential. This can be exploited by making linear approximations, so-called "quasi-active" models, of the nonlinear ionic currents (Mauro et al., 1970; Koch, 1984; Hutcheon and Yarom, 2000; Remme, 2014). In this way one can reduce the parameter space while retaining key dynamical features of the system. Results in Figures 2–7 used quasi-active currents to simplify the original, nonlinear cortical pyramidal cell model (see above) and to allow for a systematic study of the effects of active conductances on the LFP.

We here briefly describe the derivation of a quasi-active description of a single cellular compartment. The compartment includes one active current I_w that depends on the membrane potential $V(t)$ and is described by $I_w(t) = \bar{g}_w w(t)(V(t) - E_w)$, with peak conductance \bar{g}_w , reversal potential E_w , and gating variable $w(t)$. The passive leak current is given by $I_L(t) = g_L(V(t) - E_L)$, with conductance g_L and reversal potential E_L . Finally, the axial current, i.e., the net current entering or leaving to neighboring cellular compartments, is denoted by $I_{axial}(t)$. The voltage of the compartment then evolves according to

$$c_m \frac{dV(t)}{dt} = -\bar{g}_w w(t)(V(t) - E_w) - g_L(V(t) - E_L) + I_{axial}(t), \quad (1)$$

where the term $c_m \frac{dV(t)}{dt}$ is the capacitive current with membrane capacitance c_m . The dynamics of the gating variable $w(t)$ is given by

$$\tau_w(V) \frac{dw(t)}{dt} = w_\infty(V) - w(t), \quad (2)$$

with voltage-dependent activation time constant $\tau_w(V)$ and activation function $w_\infty(V)$.

The quasi-active description is obtained by linearizing V and w around resting-state values V_R and $w_\infty(V_R)$, respectively, by means of Taylor expansions. Defining the variable $m(t) \equiv (w(t) - w_\infty(V_R)) / \frac{\partial}{\partial V} w_\infty(V_R)$, we can write the linearized equation describing the voltage dynamics of a single compartment:

$$c_m \frac{dV(t)}{dt} = -g_L \left(\gamma_R (V(t) - V_R) + \mu m(t) \right) + I_{axial}(t), \quad (3)$$

where $\gamma_R \equiv 1 + \bar{g}_w w_\infty(V_R) / g_L$, i.e., the ratio between the total membrane conductance (at V_R) and the leak conductance. The parameter $\mu \equiv (\bar{g}_w / g_L) (V_R - E_w) \frac{\partial}{\partial V} w_\infty(V_R)$ determines whether the quasi-active current functions as a positive feedback (when $\mu < 0$; i.e., a regenerative current) amplifying voltage deviations from the holding potential V_R , or as a negative feedback (when $\mu > 0$; i.e., a restorative current) counteracting changes in the voltage. When $\mu = 0$, the quasi-active current is frozen and functions as a static passive current (throughout the text we will refer to this as the "passive-frozen" case). The dynamics of the linear gating variable m is described by,

$$\tau_w(V_R) \frac{dm(t)}{dt} = V(t) - V_R - m(t). \quad (4)$$

The description of the ionic currents in a single compartment is easily extended to a multi-compartmental model where each compartment can have its own set of parameters to describe the passive and quasi-active currents.

For the simulations with a single linearized h-type current or persistent sodium current (see Figure 2), we kept the passive parameters, as well as the peak conductance and activation time constant (at the specified holding potential) of the relevant active current, the same as in the original detailed model.

To systematically study the effect of the cellular distribution of a quasi-active current on the LFP (see Figure 3), we used three different channel density distributions: (1) linearly increasing with distance from the soma, (2) linearly decreasing with distance from the soma, and (3) a uniform distribution. The slopes of the increasing (decreasing) distributions were set such that the most distal tip of the apical dendrite had a sixty-fold larger (smaller) density compared to that of the soma (in line with experimental estimates for I_h distributions: Mishra and Narayanan 2015; Lörincz et al. 2002; Nusser 2009; Kole et al. 2006), and the total membrane conductance of the quasi-active current (i.e., summed over all compartments) was the same as the total

passive leak conductance g_L . The passive leak conductance was set uniformly to $50 \mu\text{S}/\text{cm}^2$ for all cases. For $w_\infty(V_R) = 0.5$ the distance-dependent quasi-active peak conductance was $\bar{g}_w(x) = 5.29 + 0.242x \mu\text{S}/\text{cm}^2$ for the linear increase, and $\bar{g}_w(x) = 143 - 0.109x \mu\text{S}/\text{cm}^2$ for the linear decrease, where the distance x was measured in μm and had a maximum of $1291 \mu\text{m}$. Note that the three distributions had the same total quasi-active membrane conductance summed over the neuronal membrane.

The parameters μ and γ_R vary along the cell for the non-uniform channel distributions. We introduced $\mu^* \equiv \mu(x)g_L/\bar{g}_w(x)$, such that $\mu^* = (V_R - E_w)\frac{\partial}{\partial V}w_\infty(V_R)$ is independent of the distribution of the quasi-active conductance and can be specified as a single constant. We used $\mu^* = -0.5$ for the regenerative conductance, $\mu^* = 0$ for the passive-frozen conductance, and $\mu^* = 2$ for the restorative conductance. For the uniform distribution this gives the same values as those used in Remme and Rinzel (2011), namely $\mu = -1, 0, 4$ for the regenerative, passive-frozen and restorative cases, respectively. The activation time constant $\tau_w(V_R)$ of the quasi-active conductance was set to 50 ms (unless specified otherwise) in order to have dynamics similar to the h-type conductance. The intracellular resistivity was $R_a = 100 \Omega\text{cm}$, and the specific membrane capacitance $c_m = 1 \mu\text{F}/\text{cm}^2$.

Calculation of extracellular potentials

Extracellular potentials recorded inside the brain are generated by transmembrane currents from cells in the vicinity of the electrode contact (Nunez and Srinivasan, 2006). The biophysical origin of the recorded signals is well understood in the context of volume conduction theory. Extracellular potentials originating from a simulated multi-compartmental neuron model can be computed by first obtaining the transmembrane currents $I_n(t)$ from each compartment n at position \vec{r}_n . Next, the extracellular potential $\phi(\vec{r}, t)$ at position \vec{r} resulting from these transmembrane currents can be calculated (Holt and Koch, 1999; Lindén et al., 2014):

$$\phi(\vec{r}, t) = \frac{1}{4\pi\sigma} \sum_{n=1}^N I_n(t) \int \frac{d\vec{r}_n}{|\vec{r} - \vec{r}_n|}, \quad (5)$$

where σ is the conductivity of the extracellular medium. This corresponds to the so-called line-source formula assuming the transmembrane currents to be evenly distributed along the axes of cylindrical neural compartments, see Lindén et al. (2014) for a detailed description.

All simulations and computations of the extracellular potentials were carried out using LFPy (Lindén et al., 2014), an open-source Python package that provides an interface to NEURON (Carnevale and Hines, 2006). The time step of the neural simulation was 0.0625 ms . For all simulations the first 1000 ms was discarded to avoid initialization effects. All simulation code used to produce the figures in this study are available upon request.

Results

To examine the contribution of subthreshold, active conductances on the extracellular potential we started by considering a previously published, detailed model of a layer 5 cortical pyramidal neuron endowed with a large variety of active conductances (Hay et al., 2011; see Methods).

Note that the term LFP commonly refers to the low-pass filtered version (below 300-500 Hz) of the extracellular potential (to filter away spikes). Since there is no spiking activity in the present use of the model, we simply refer here to the unfiltered version of the extracellular potential as the LFP.

Active subthreshold conductances shape the LFP

We first determined the LFP in response to a single excitatory synaptic input. We compared the LFP signal of the active neuron model with a passive version of the model (i.e., all active conductances removed). The synaptic input was provided either to the distal apical dendrite (Figure 1A, top row) or to the soma (Figure 1A, bottom row) while the entire cell was hyperpolarized to -80 mV (Figure 1A, left column) or depolarized to -60 mV (Figure 1A, right column). The LFP was calculated at five different positions outside the neuron (marked by cyan dots). The difference between the LFPs of the active and passive models depended on the holding potential of the cell, the synaptic input position, as well as the extracellular recording position. In particular, we observed for hyperpolarized potentials that the active and passive LFPs were markedly different for apical synaptic input, while being very similar for somatic input.

In order to more fully characterize the effects of active currents on the LFP we next applied white-noise current input instead of a single synaptic input, and determined the power spectral density (PSD) of the resulting LFP (i.e., the square of the Fourier amplitude of the signal as a function of frequency). The white-noise input current had equal signal power at all integer frequencies in the considered frequency range (1–500 Hz; see also Lindén et al., 2010). At most extracellular recording positions, a low-pass filtering was observed in the LFP of both the active and the passive model. This results from the intrinsic dendritic filtering (see, e.g., Pettersen et al., 2012; Lindén et al., 2010; Pettersen and Einevoll, 2008) and increases with distance from the synaptic input site (Figure 1B). The most striking difference between the active and the passive case was again found for the cell in a hyperpolarized state with apical input (Figure 1B, top left), which showed a strong resonance (i.e., band-pass filter with a peak around 17–22 Hz) for the active model LFP, but not for the passive one. Note that the cell in a depolarized state and apical input shows qualitatively the same effect, though less prominent (Figure 1B, top right).

While the main effect of the active conductances in the case of apical input was to reduce the LFP power at the lowest frequencies, the effect from active conductances on somatic input

was qualitatively different. For the cell with a depolarized resting potential, white-noise current resulted in an amplification of the low frequencies (Figure 1B, bottom right). In all situations considered, a difference between the active and passive model was only apparent below about 30–50 Hz. At higher frequencies, capacitive currents dominated the transmembrane return currents both in the active and passive models (Lindén et al., 2010). The exact cross-over frequency where the capacitive currents become dominant over the ionic membrane currents, depends on neuronal properties (e.g., ion channel densities), as well as the positions of the input and the recording electrode.

Which ionic currents in the model are responsible for the large difference between the active and passive model for hyperpolarized potentials and with apical input? One obvious candidate is the hyperpolarization-activated inward current I_h . This current operates at subthreshold voltages, is concentrated in the apical dendrites, and dampens the lowest frequency components of the membrane potential response to input (Magee, 1998; Hu et al., 2009, 2002; Kole et al., 2006; Almog and Korngreen, 2014). Indeed, we found that when we extended the passive model with only the h-type conductance, the LFP was indistinguishable from the full active model when the cell was in a hyperpolarized state and received apical input (Figure 1C).

Two effects are involved in the reduction of the LFP signal power at low frequencies in the model with I_h . First, with an additional active current comes an increased membrane conductance, which shifts the transmembrane return currents associated with the input current closer to the input position on the neuron. This gives smaller current-dipole moments and thus generally smaller LFPs (Pettersen and Einevoll, 2008; Lindén et al., 2010; Pettersen et al., 2012). This is still a passive-membrane effect and can simply be incorporated into a passive model by rescaling the leak conductance corresponding to adding a "frozen" h-type conductance. The second effect stems from the dynamical properties of an active conductance such as I_h , which actively counteract voltage fluctuations at low frequencies. While the extension of the passive model with a "frozen I_h " was found to strongly dampen the low-frequency components of the LFP compared to the full active case (Figure 1C, gray dotted lines), it failed to reproduce the resonance of the models with the dynamic I_h conductance (blue dashed and red). This demonstrates that the resonance observed in the LFP was an effect caused by the dynamics of the h-type channels, similar to previously reported I_h -induced resonances in the membrane potential (Hutcheon and Yarom, 2000; Hu et al., 2009; Zhuchkova et al., 2013).

Linear models capture the effects of active conductances on the LFP in the subthreshold regime

Above, we established that the h-type conductance is key in shaping the LFP for subthreshold input to the apical dendrites in the model by Hay et al. (2011). Because in reality there is considerable variation between neurons regarding their biophysical properties, and perhaps not

all relevant subthreshold currents were captured by this specific model, we next set out to perform a systematic study of the effects that any subthreshold active conductance can have on the LFP. For this we made use of the so-called "quasi-active" approximation of voltage-dependent currents. Active membrane conductances in general exhibit nonlinear behavior, but for small deviations of the membrane potential around a holding potential, active conductances often behave in a near-linear fashion. The dynamics of an active conductance can then be approximated by linearizing the current around a holding potential (Mauro et al., 1970; Koch, 1984; Remme and Rinzel, 2011; Remme, 2014; see Methods). This retains the voltage-dependent current dynamics for potentials not too far away from that potential, while strongly reducing the parameter space of the model and allowing an intuitive understanding of the model behavior.

Linearized active conductances can be divided into two classes: restorative and regenerative. Restorative conductances dampen the lowest frequency components of the membrane potential response to synaptic input, also leading to narrower synaptic voltage responses (Remme and Rinzel, 2011). The intrinsic low-pass filtering of the cellular membrane (Koch, 1999), in combination with the active dampening of low frequencies (i.e., high-pass filtering) by restorative conductances, can thus cause a resonance in the membrane potential PSD (Remme and Rinzel, 2011; Zhuchkova et al., 2013; Hu et al., 2009). Examples of restorative currents are the h-current and the M-type slow potassium current. In contrast, regenerative conductances amplify the low-frequency components of the membrane potential response to synaptic input, making the voltage responses to synaptic input broader in time as they propagate along the dendrites. This will only add to the intrinsic low-pass filtering of the cellular membrane, and as such, regenerative conductances lack the easily recognizable feature of the restorative conductances. Examples of regenerative conductances are the persistent sodium current I_{NaP} and the low-voltage activated calcium current (Remme and Rinzel, 2011).

It is well established that quasi-active approximations of active currents can accurately capture the subthreshold effects on the membrane potential (Koch, 1984; Remme and Rinzel, 2011). To test whether this conclusion also holds for the LFP, we started with the original cortical pyramidal cell model from Hay et al. (2011), and simplified it to two separate cases with only a single active conductance remaining in each. For the first case, we kept only the restorative I_h conductance, with its increasing conductance along the apical dendrite away from the soma. The resting potential was set uniformly to the hyperpolarized potential of -80 mV and the cell was stimulated with apical white-noise input. In the second case we kept only the regenerative persistent sodium current, solely present in the soma, set the resting potential uniformly to the depolarized potential of -60 mV, and applied somatic white-noise input. The I_h -only model yielded the resonance in the LFP that was discussed above (Figure 2A, blue dashed lines), while the I_{NaP} -only model gave an amplification of the low-frequency components of the LFP (Figure 2B, pink dashed lines). We then simulated the models with linearized versions of the original conductances and found the LFP from the active and linearized conductances to be

indistinguishable (Figure 2, blue versus green, pink versus orange). In fact, for all tested combinations of resting potentials, input positions, and LFP recording positions, the quasi-active approximation was found to faithfully reproduce the signature of the active conductance in the membrane potentials, the transmembrane currents, as well as in the LFP. This applied as long as the perturbations of the membrane potential around the resting potential were not too large. For I_h , fluctuations of 10–15 mV are typically within the appropriate range (data not shown, but see, e.g., Remme and Rinzel, 2011). We conclude that systematic studies with a single quasi-active conductance are justified.

Spatially asymmetric distributions of ion channels and inputs enhance the effect of active currents on the LFP

We next turned to a systematic exploration of how active subthreshold currents affect the LFP. For this we used a pyramidal cell model with a single quasi-active current. The key parameter characterizing the quasi-active current is μ^* , the sign of which determines whether the current is regenerative ($\mu^* < 0$) or restorative ($\mu^* > 0$), while $\mu^* = 0$ for a passive-frozen conductance (i.e., the added conductance has no dynamics and thus simply adds to the passive leak conductance). The quasi-active current was distributed across the cell either uniformly, linearly increasing with distance from soma, or linearly decreasing with distance from soma (Figure 3 – left, middle and right columns, respectively). In all cases the models had the same total membrane conductance summed over the neuronal membrane. We applied white-noise current input either to the apical dendrite (panel B) or to the soma (panel C) and calculated the LFP-PSD for each case in the apical region and in the somatic region. A large difference between the results from the passive-frozen model and the restorative or regenerative models would imply that the dynamics of the active conductance in question shapes the LFP. Indeed, we found for most scenarios, that the regenerative current caused an amplification of the low-frequency components of the LFP (Figure 3, red lines) compared to the passive-frozen case (black line), while a restorative current dampened the low frequencies, leading to the previously discussed resonance (Figure 3, blue lines). However, as discussed below, there were exceptions.

We found that the impact of the quasi-active current was always largest in the LFP recorded on the opposite side of the cell compared to the position of the input, i.e., next to the soma for apical input (panel B, bottom row) and next to the apical dendrite for somatic input (panel C, top row). This can be understood since the LFP is a distance-weighted sum of all transmembrane currents, so that transmembrane currents close to the recording electrode will contribute more to the measured LFP signal. For recordings on the opposite side relative to the input, the transmembrane return currents have been strongly affected by the active conductance after propagating along the apical dendrite. The effect was also largest when the quasi-active current was non-uniformly distributed and concentrated at the position of the input (panel B, middle

column; panel C, right column), and smallest when the input was to a region of low density (panel B, right column; panel C, middle column). This also follows from the reasoning above: when the input is to a region with a low density of an active current, the return currents close to the input will be hardly affected by the active current. As the signal propagates along the dendrites to regions with higher densities of the active current, it will be increasingly affected by the active current, however, the signal amplitude will also gradually decrease. Therefore, the LFP is less affected by the presence of a non-uniformly distributed active current when the input is provided to a region with low densities compared to when input is provided to a high-density region.

Besides the type of an active current (i.e., restorative or regenerative) and how it is distributed across the neuron, also its activation time constant is key for the effects on the LFP. The dynamics of an active current will only express its effect on the membrane potential, transmembrane currents and LFP for frequencies that are sufficiently low relative to the activation time constant ($\tau_w(V_R)$). This is seen by considering different activation time constants for the quasi-active conductance (Figure 4). Increasing the activation time constant decreased the frequency at which the regenerative/restorative responses became similar to the passive-frozen case. For the resonance this means that its peak becomes broader and shifts to lower frequencies for larger activation time constants.

Resonance is expressed for asymmetrically distributed synaptic input

In the above simulations we considered a single white-noise current input to characterize the effect of active currents on the LFP. We next examined whether the observed effects also hold when the cell receives a barrage of synaptic input as is typical for *in vivo* conditions (Destexhe et al., 2003).

We considered a cell model with a single quasi-active conductance that increases linearly in density with distance from the soma. The model received input from 1000 excitatory synapses that were distributed across the neuronal membrane and randomly activated according to independent Poisson statistics. We considered three synaptic distributions: (1) uniformly distributed across the distal apical tuft dendrites located more than 900 μm from the soma (Figure 5A), (2) uniformly distributed across the apical dendrites more than 600 μm from the soma (Figure 5B), and (3) uniformly across the entire cell (Figure 5C). For each distribution the exact same 1000 synapse positions and input spike trains were used in the simulations for the regenerative, passive-frozen, and restorative conductances. Hence, the only difference between the simulations with a given synapse distribution was the nature of the quasi-active conductance.

The resonance for the restorative model was clearly retained for LFP signals recorded close to the soma when the synaptic inputs were distributed asymmetrically, being concentrated in the apical dendrites (Figure 5A,B). However, for uniformly distributed input (Figure 5C) the

resonance was practically undetectable. Similarly, for the regenerative model, increases of low frequencies in the LFP-PSD were only reliably observed for the models with asymmetric synaptic input distributions (Figure 5A,B). Note that we obtained the same results when keeping the synapse densities fixed across the three synapse distributions, instead of keeping the total synapse number constant (results not shown). The dependence of the modulation of the LFP on the input distribution can be understood by considering the results in Figure 3: the case with uniform input approximately corresponds to a linear combination of the LFPs stemming from apical and somatic input (Figure 3, middle column). In the somatic region the net LFP signal will be strongly dominated by the transmembrane currents resulting from the somatic input, which are hardly affected by the active conductances since these are concentrated in the distal apical dendrites.

Resonance is a spatially stable feature in the LFP

The LFP signals measured in *in vivo* experiments are generated by many neurons located within a distance from a few hundred micrometers up to a few millimeters away from the recording electrode (Lindén et al., 2011; Łęski et al., 2013). An effect of a quasi-active conductance on the LFP generated by a single neuron will only carry over to the LFP generated by an entire population if the effect is spatially "robust". For example, the resonance of the single-neuron LFP will only be observed in the population-LFP if it is present in a sizable part of the volume surrounding the cell. If it would only be recorded at special electrode positions, then it would be expected to average out when considering an entire population. The linearity of the LFP signal generation implies that the summed contributions of many single neuron-LFP signals with similar shape, would result in a population LFP with a similar shape. It is therefore key to study how the LFP varies in the space around the neuron.

We calculated the LFP at a dense grid of positions around a pyramidal cell receiving apical white-noise input (Figure 6). The model expressed a restorative quasi-active conductance that increased in density with distance from the soma. Our previous results (see Figure 3) demonstrated that such a model can show strong resonances in the LFP. The maximum amplitude of the LFP-PSD on the position-grid around the cell had the shape of a dipole (panel A), as expected following the requirement of charge conservation (Lindén et al., 2010). This dipolar nature of the LFP pattern was also demonstrated by comparing two normalized LFP time traces at opposite sides of the zero-crossing region of the dipole and noting that they are almost mirror images (panel B; depicted traces correspond to first and third electrode contacts from the top in the first column in panel A).

For two columns of electrode positions (marked in panel A) we examined the LFP-PSD in detail (panel C). The LFP signals again demonstrated that the resonance was most pronounced on the side of the cell opposite to the input (compare lightest trace to the darker ones). Note that

the electrodes positioned in the zero-crossing region of the dipole exhibited more variable PSD shapes, for example, a strong band-stop at around 20 Hz. This is because different frequency components of the LFP will have slightly different zero-crossing regions (see also Lindén et al. 2010). We focused on the LFP resonance and determined the frequency of maximum LFP power for the grid of positions around the neuron. The peak frequency was found to be stable at around 20 Hz, except in the zero-crossing region of the dipole (panel D).

The so-called Q-value is commonly used to characterize resonances. In the neurophysiological literature it is often defined as the magnitude of a variable (typically the membrane potential) at the resonance frequency divided by its value at the lowest frequency considered (Hutcheon et al., 1996). We found that the LFP Q-value was stable and large at the soma region of the cell (panel E), i.e., on the side opposite to the input, in accordance with observations from Figures 1–3. Note that the largest LFP Q-values were in fact observed in the zero-crossing region. However, in this region it does not reflect a resonance caused by a restorative current, but rather the very variable LFP pattern in this region. The lower signal power in this region (Figure 6A), in combination with the fact that the position of the zero-crossing region will depend on various parameters, such as the exact position of the synaptic input, means that the very large Q-values seen here will not carry over to the population LFP.

Spatial profile of the membrane potentials, transmembrane currents and LFP

Above we demonstrated an amplification and a dampening of low-frequency LFP components caused by regenerative and restorative conductances, respectively. These effects were qualitatively similar to the effects of such active conductances on the membrane potential as reported by, for example, Remme and Rinzel (2011). However, as LFP signals reflect transmembrane currents, it is a fundamentally different measure of neural activity than the membrane potential (Pettersen et al., 2012; Einevoll et al., 2013a). It can therefore not be expected *a priori* that quasi-active conductances always have qualitatively similar effects on the LFP and the membrane potential. We thus next studied the differences in the effects of active currents on the membrane potential, transmembrane currents and LFP in a simplified setting, i.e., white-noise current input injected into a single, long neurite with uniform passive membrane parameters and a single uniformly distributed quasi-active conductance.

Focusing first on the membrane potential (V_m , Figure 7A), we indeed observe that the low-frequency components are always amplified by regenerative currents (red), whereas they are always dampened by restorative conductances (blue), compared to the passive-frozen case (black). The effects increase with "exposure" to the quasi-active current, i.e., how far the input has propagated along the neurite (Remme and Rinzel, 2011). In addition, the membrane potential is increasingly low-pass filtered with distance, resulting in a stronger membrane-potential

resonance with distance from the input site.

The position dependence of transmembrane currents is more complicated (I_m , panel B). We first consider the passive-frozen case: at the input site (panel B, leftmost) the transmembrane current is approximately equal for all frequencies, as expected due to the white-noise current input. From charge conservation it follows that the current that enters the cell must also exit the cell, i.e., that transmembrane currents across the neuron sum to zero (Koch, 1999). Since high-frequency components propagate less than low-frequency components, they dominate close to the input. Hence, the transmembrane currents show a high-pass filtered PSD at positions close to the white-noise input (panel B, second column). The reverse is true far away from the input (panel B, rightmost), where there is a low-pass effect similar as for the membrane potential. This results from the stronger propagation of the low frequencies, which therefore dominate over the high frequencies at larger distances (Koch, 1999; Lindén et al., 2010). Note that at intermediate distances, a “passive resonance” (panel B, third column) can be observed through the combination of a low-pass and a high-pass filter.

A restorative current functions as a negative feedback, counteracting membrane potential changes, such that voltage signals do not spread as far down the neurite as in the passive-frozen case (panel A; compare blue and black traces). Therefore the return currents resulting from the current injections move closer to the input site, leading to an amplification of the transmembrane currents close to the input site, and a decrease far away from the input site, relative to the passive-frozen case (panel B).

Regenerative currents amplify membrane potential deviations along the neurite (panel A; compare red and black traces) and thus shift the return currents further away from the input compared to the passive-frozen case. This leads to a decrease in the transmembrane currents close to the input site, and an amplification far away from the input site compared to the passive-frozen case (panel B).

Because the LFP signal is a distance-weighted sum of all transmembrane currents, the described effects in the transmembrane currents are all present in the LFP measured very close to the neurite (panel C; 20 μm). For electrodes further away from the neurite (panel D; 300 μm) the LFP is no longer dominated by transmembrane currents from any single part of the neurite. Since the restorative currents move the transmembrane return currents closer to the input site, a smaller current dipole moment is generated, thus resulting in a decrease of the LFP-power at most recording positions. The opposite is found for the model with a regenerative conductance. As we demonstrated in Figure 4, these effects hold for the low-frequency components of the LFP, because the dynamics of the active current only affect the cell response for frequencies that are slow compared to the activation time constant.

The resulting transmembrane currents from a single white-noise input into a neurite also helps explain why we needed asymmetric input to retain the effects that an active current has on the LFP-PSD (see Figure 5). For a single input location, the effects of an active current on

the low-frequency components of the transmembrane currents close to, and far away from the white-noise input were opposite (Figure 7B, second versus fourth panel). Hence, for input that is localized to one region of a cell, the contributions from active currents will sum "constructively" and largely retain the characteristic LFP signatures for a single individual synaptic input. For uniform input, however, an active current will give a combination of amplifying and dampening effects which will sum "destructively", decreasing the total effect of the active current on the shape of the LFP.

Discussion

In the present paper we explored the role played by active conductances in shaping the local field potential (LFP) generated by neurons. It thus goes beyond previous principled studies on the LFP generated by synaptically activated passive neurons (Lindén et al., 2010, 2011; Łęski et al., 2013). While the various effects of active conductances in forming the LFP have previously been explored in comprehensive network simulations of thousands of spiking neurons (Reimann et al., 2013), the present work was instead tailored to probe subthreshold effects in detail.

With a morphologically detailed and experimentally constrained cortical pyramidal cell model, we demonstrated that active conductances can strongly shape the LFP stemming from subthreshold input. The precise effects depended on the position of the input, the position of the extracellular electrode, and the membrane potential of the cell (Figure 1). The subthreshold active conductances had distinct effects on the power spectral density (PSD) of the LFP, providing either amplification or attenuation of the low frequencies, in the latter case leading to a resonance in the LFP-PSD. The effects on the LFP were observed for various spatial distributions of the active conductances across the cell, but generally required an asymmetric distribution of synaptic input onto the cell (Figure 5). We found that the effect of a subthreshold active conductance on the LFP was maximized for (i) an asymmetric distribution of the active conductance, (ii) when the input was targeted to regions where the active conductance was most strongly expressed, and (iii) the LFP was recorded on the opposite side of the cell with respect to the input (Figure 3).

Peaks in the LFP-PSD are commonly observed experimentally (see, e.g., Roberts et al., 2013; Hadjipapas et al., 2015), and such peaks are usually interpreted as the result of network oscillations, i.e., oscillatory firing activity driving the LFP-generating neurons (Buzsáki and Draguhn, 2004). Importantly, our work shows that such peaks may also be due to subthreshold restorative conductances molding the transmembrane return currents. In particular, in our simulations with the pyramidal cell model by Hay et al. (2011) we found that the h-type current had a prominent role in shaping the LFP and could cause a strong resonance in the LFP-PSD (Figures 1C, 2A). The h-type current is strongly expressed in cortical and hippocampal pyramidal neurons and has a particularly asymmetric distribution across the cell, increasing in density

along the apical dendrites and peaking in the distal apical tuft dendrites (Magee, 1998; Williams and Stuart, 2000; Harnett et al., 2015). The h-type current can be expected to impact the LFP resulting from synaptic input that is predominantly targeting the apical dendritic tuft of populations of cortical or hippocampal pyramidal neurons. Indeed, various input pathways to pyramidal neurons target specific domains of the cell (see, e.g., Petreanu et al., 2009). An intriguing consequence of our work is that the LFP can contain information on the spatial distribution of subthreshold active channels, as well as on the location of synaptic input to the LFP generating cells. For example, given a known apical concentration of h-type conductances, a resonance in the LFP due to I_h would suggest that the cells receive asymmetric input. Vice versa, if asymmetrical input is provided, an absence of a resonance in the LFP (measured at multiple locations along the cell axis) suggests that the cell does not strongly express restorative currents.

A direct approach to test our model predictions would be through *in vitro* cortical slice experiments. The asymmetric input can be provided by targeting the apical dendrites using, e.g., glutamate uncaging. The polarized distribution of I_h that pyramidal neurons typically display, should then give rise to a notable resonance in the LFP-PSD, in particular when measured close to the pyramidal cell soma (Figure 6). Addition of an I_h blocker (e.g., ZD7288) is expected to remove any resonance caused by I_h .

In most of our simulations we described voltage-dependent channels with so-called quasi-active currents, which are linear approximations of the voltage-dependent currents (Mauro et al., 1970; Koch, 1984; Hutcheon and Yarom, 2000; Remme, 2014). The linear descriptions highlights that there are basically two types of active currents: regenerative and restorative, which have opposite effects on the voltage response, amplifying or counteracting voltage deflections, respectively. The quasi-active description not only permits the use of various analytical techniques for linear systems, but also strongly reduces the number of parameters to describe an active current. This simplified description enables the systematic study of the effect of subthreshold input on the voltage response of active, dendritic neurons and allows a thorough understanding of the dynamics of the system (Koch, 1984; Bressloff, 1999; Coombes et al., 2007; Goldberg et al., 2007; Remme et al., 2009, 2010; Remme and Rinzel, 2011). We showed here that the quasi-active current descriptions can also be used to accurately capture the LFP signal (Figure 2). Because the h-type current was dominating the subthreshold effects on the LFP in the model by Hay et al. (2011), a single quasi-active current was sufficient to approximate the LFP signal of the full, nonlinear model. The approach enabled us to establish an overview of the effects of active currents on the LFP signal. We achieved this by using the detailed neuron morphology with a single quasi-active current, where the current was either restorative or regenerative, had a range of activation time constants (Figure 4), and was distributed in various ways across the cell (Figure 3).

In the *in vivo* situation, the measured LFP will reflect the activity in populations of neurons (Einevoll et al., 2013a). A natural extension of the present work will be to investigate

the effect of active dendritic currents on the LFP in a population of neurons receiving synaptic inputs (Lindén et al., 2011; Łęski et al., 2013). For the case of passive dendrites the key factor in determining the magnitude and spread of the population LFP was found to be the amount of correlation between the numerous synaptic inputs driving the population (Lindén et al., 2011; Einevoll et al., 2013a; Łęski et al., 2013). The synaptic correlation level will be expected to also be key for determining the population LFP in the case of active dendritic conductances, but insight into its specific influence will require detailed modeling studies. A key simplifying feature of the present study was the observation that linearized quasi-active conductances accounted very well for the salient effects of active subthreshold conductances on the single-neuron LFP. This approximation will also be applicable when studying effects of subthreshold active conductances on population LFPs, thus assuring linearity of the model system and greatly simplifying the analysis as in Lindén et al. (2011) and Łęski et al. (2013).

In the present study we have not considered suprathreshold active conductances, i.e., the active channels underlying spike generation. While the present biophysical modeling scheme is equally applicable to spikes (Holt and Koch, 1999; Gold et al., 2006; Pettersen and Einevoll, 2008), the contributions to the LFP from such spikes may be expected to be negligible for cortical networks in the *in vivo* situation, at least for the low frequencies of LFP. In Pettersen et al. (2008) the extracellular potential generated by a synaptically-activated population of 1040 pyramidal neurons mimicking a layer-5 population in rat somatosensory (barrel) cortex was modeled by the present biophysical scheme. In order for the model predictions to be in accordance with measured extracellular potentials from the rat barrel cortex, both for the LFP (frequencies \lesssim 500 Hz) and for multi-unit activity (frequencies \gtrsim 500 Hz), only 4% (40 of 1040) of the model neurons were tuned to fire an action potential following the stimulus input. In this situation the modeled LFP signal was observed to be completely dominated by the synaptic input currents and their associated return currents, with negligible contributions from the spikes themselves. However, in situations with strongly correlated firing, for example during sharp-wave ripples in hippocampus, the spikes have been found to have sizable contributions to the extracellular potentials for frequencies down to 100 Hz (Schomburg et al., 2012; see also Reimann et al., 2013; Taxidis et al., 2015). For further discussion on the biophysical origin of the extracellular potentials in this "high-gamma" range, see for example Ray and Maunsell (2011) and Scheffer-Teixeira et al. (2013). Note also that as the extracellular potential is given as a linear sum of contributions from the various transmembrane currents surrounding the contact, putative contributions from spikes can be estimated by adding computed spike signatures (Holt and Koch, 1999; Gold et al., 2006; Pettersen and Einevoll, 2008) to the present results for the LFP.

Even though the LFP has been measured for more than half a century, the interpretation of the recorded data has so far largely been qualitative (for a review, see Einevoll et al., 2013a). We believe that the present investigation on the role of active dendritic conductances in shaping the recorded signal, will turn out to be an important contribution towards the goal of making

combined modeling and measurement of the LFP signal a practical research tool for detailed probing of neural circuit activity.

Competing Interests

The authors declare no competing financial interests.

Funding

The research leading to these results has received funding from the European Union Seventh Framework Program (FP7/2007-2013) under grant agreement 604102 (Human Brain Project, HBP), the Research Council of Norway (NevroNor, Notur, nn4661k), the Norwegian node of the International Neuroinformatics Coordinating Facility (INCF, NFR 214842/H10), and the Einstein Foundation Berlin.

Author contributions

All authors took part in designing the work, interpreting data, and writing the manuscript. TVN wrote the simulation code. TVN and MWHR made the figures. All authors approved the final version of the manuscript and agree to be accountable for all aspects of the work in ensuring that questions related to the accuracy or integrity of any part of the work are appropriately investigated and resolved. All persons designated as authors qualify for authorship, and all those who qualify for authorship are listed.

References

- Almog M & Korngreen A (2014). A quantitative description of dendritic conductances and its application to dendritic excitation in layer 5 pyramidal neurons. *J Neurosci* **34**, 182–96.
- Bressloff PC (1999). Resonantlike synchronization and bursting in a model of pulse-coupled neurons with active dendrites. *J Comput Neurosci* **6**, 237–249.
- Buzsáki G, Anastassiou CA & Koch C (2012). The origin of extracellular fields and currents—EEG, ECoG, LFP and spikes. *Nat Rev Neurosci* **13**, 407–20.
- Buzsáki G & Draguhn A (2004). Neuronal Oscillations in Cortical Networks. *Science* **304**, 1926–1930.
- Carnevale NT & Hines ML (2006). *The NEURON Book*. Cambridge University Press, Cambridge, UK.
- Coombes S, Timofeeva Y, Svensson CM, Lord GJ, Josić K, Cox SJ & Colbert CM (2007). Branching dendrites with resonant membrane: a "sum-over-trips" approach. *Biol Cybern* **97**, 137–149.
- Destexhe A, Rudolph M & Paré D (2003). The high-conductance state of neocortical neurons in vivo. *Nat Rev Neurosci* **4**, 739–751.
- Einevoll GT, Kayser C, Logothetis N & Panzeri S (2013a). Modelling and analysis of local field potentials for studying the function of cortical circuits. *Nat Rev Neurosci* **14**, 770–785.
- Einevoll GT, Lindén H, Tetzlaff T, Łęski S & Pettersen KH (2013b). Local field potentials - biophysical origin and analysis. In Quiroga RQ & Panzeri S, editors, *Principles of Neural Coding*, chapter 3, pp. 37–60. CRC Press, Boca Raton, FL.
- Einevoll GT, Pettersen KH, Devor A, Ulbert I, Halgren E & Dale AM (2007). Laminar population analysis: estimating firing rates and evoked synaptic activity from multielectrode recordings in rat barrel cortex. *J Neurophysiol* **97**, 2174–2190.
- Gold C, Henze Da, Koch C & Buzsáki G (2006). On the origin of the extracellular action potential waveform: A modeling study. *J of Neurophysiol* **95**, 3113–28.
- Goldberg JA, Deister CA & Wilson CJ (2007). Response properties and synchronization of rhythmically firing dendritic neurons. *J Neurophysiol* **97**, 208–219.
- Hadjipapas A, Lowet E, Roberts M, Peter A & De Weerd P (2015). Parametric variation of gamma frequency and power with luminance contrast: A comparative study of human MEG and monkey LFP and spike responses. *NeuroImage* **112**, 327–340.

- Harnett MT, Magee JC & Williams SR (2015). Distribution and Function of HCN Channels in the Apical Dendritic Tuft of Neocortical Pyramidal Neurons. *J Neurosci* **35**, 1024–1037.
- Hay E, Hill S, Schürmann F, Markram H & Segev I (2011). Models of neocortical layer 5b pyramidal cells capturing a wide range of dendritic and perisomatic active properties. *PLoS Comp Biol* **7**, 1–18.
- Holt GR & Koch C (1999). Electrical interactions via the extracellular potential near cell bodies. *J Comput Neurosci* **6**, 169–184.
- Hu H, Vervaeke K & Storm JF (2002). Two forms of electrical resonance at theta frequencies, generated by M-current, h-current and persistent Na⁺ current in rat hippocampal pyramidal cells. *J Physiol* **545**, 783–805.
- Hu H, Vervaeke K, Graham LJ & Storm JF (2009). Complementary theta resonance filtering by two spatially segregated mechanisms in CA1 hippocampal pyramidal neurons. *J Neurosci* **29**, 14472–83.
- Hu H, Vervaeke K & Storm JF (2007). M-channels (Kv7/KCNQ channels) that regulate synaptic integration, excitability, and spike pattern of CA1 pyramidal cells are located in the perisomatic region. *J Neurosci* **27**, 1853–1867.
- Hutcheon B, Miura RM & Pail E (1996). Models of subthreshold membrane resonance in neocortical neurons. *J Neurophysiol* **76**, 698–714.
- Hutcheon B & Yarom Y (2000). Resonance, oscillation and the intrinsic frequency preferences of neurons. *Trends Neurosci* **23**, 216–22.
- Koch C (1984). Cable Theory in Neurons with Active, Linearized Membranes. *Biol Cybern* **33**, 15–33.
- Koch C (1999). *Biophysics of Computation* Oxford Univ Press, Oxford.
- Kole MHP, Hallermann S & Stuart GJ (2006). Single I_h channels in pyramidal neuron dendrites: properties, distribution, and impact on action potential output. *J Neurosci* **26**, 1677–87.
- Łęski S, Lindén H, Tetzlaff T, Pettersen KH & Einevoll GT (2013). Frequency dependence of signal power and spatial reach of the local field potential. *PLoS Comp Biol* **9**, 1–23.
- Lindén H, Hagen E, Łęski S, Norheim ES, Pettersen KH & Einevoll GT (2014). LFPy: a tool for biophysical simulation of extracellular potentials generated by detailed model neurons. *Front Neuroinform* **7**, 1–15.

- Lindén H, Pettersen KH & Einevoll GT (2010). Intrinsic dendritic filtering gives low-pass power spectra of local field potentials. *J Comput Neurosci* **29**, 423–44.
- Lindén H, Tetzlaff T, Potjans TC, Pettersen KH, Grün S, Diesmann M & Einevoll GT (2011). Modeling the Spatial Reach of the LFP. *Neuron* **72**, 859–72.
- Lörincz A, Notomi T, Tamás G, Shigemoto R & Nusser Z (2002). Polarized and compartment-dependent distribution of HCN1 in pyramidal cell dendrites. *Nat Neurosci* **5**, 1185–1193.
- Magee JC (1998). Dendritic hyperpolarization-activated currents modify the integrative properties of hippocampal CA1 pyramidal neurons. *J Neurosci* **18**, 7613–24.
- Major G, Larkum ME & Schiller J (2013). Active properties of neocortical pyramidal neuron dendrites. *Annu Rev Neurosci* **36**, 1–24.
- Mauro A, Conti F, Dodge F & Schor R (1970). Subthreshold behavior and phenomenological impedance of the squid giant axon. *J Gen Physiol* **55**, 497–523.
- Mishra P & Narayanan R (2015). High-conductance states and A-type K⁺ channels are potential regulators of the conductance-current balance triggered by HCN channels. *J Neurophysiol* **113**, 23–43.
- Mitzdorf U (1985). Current Source-Density Method and Application in Cat Cerebral Cortex: Investigation of Evoked Potentials and EEG Phenomena. *Physiol Rev* **65**.
- Nunez PL & Srinivasan R (2006). *Electric Fields of the Brain*, Oxford University Press, New York.
- Nusser Z (2009). Variability in the subcellular distribution of ion channels increases neuronal diversity. *Trends Neurosci* **32**, 267–274.
- Petreaun L, Mao T, Sternson SM & Svoboda K (2009). The subcellular organization of neocortical excitatory connections. *Nature* **457**, 1142–1145.
- Pettersen KH, Lindén H, Dale AM & Einevoll GT (2012). Extracellular spikes and CSD. In Brette R & Destexhe A, editors, *Handbook of Neural Activity Measurement*, chapter 4, pp. 92–135. Cambridge University Press, Cambridge, UK.
- Pettersen KH & Einevoll GT (2008). Amplitude variability and extracellular low-pass filtering of neuronal spikes. *Biophys J* **94**, 784–802.
- Pettersen KH, Hagen E & Einevoll GT (2008). Estimation of population firing rates and current source densities from laminar electrode recordings. *J Comput Neurosci* **24**, 291–313.

- Rall W & Shepherd G (1968). Theoretical reconstruction dendrodendritic of field potentials and in olfactory bulb synaptic interactions. *J Neurophysiol* **31**, 884–915.
- Ray S & Maunsell JHR (2011). Different origins of gamma rhythm and high-gamma activity in macaque visual cortex. *PLoS Biol* **9**, 1–15.
- Reimann M, Anastassiou C, Perin R, Hill SL, Markram H & Koch C (2013). A Biophysically Detailed Model of Neocortical Local Field Potentials Predicts the Critical Role of Active Membrane Currents. *Neuron* **79**, 375–390.
- Remme MWH (2014). Quasi-active approximation of nonlinear dendritic cables In Jaeger D & Jung R, editors, *Encyclopedia of Computational Neuroscience*, pp. 1–5. Springer New York.
- Remme MWH, Lengyel M & Gutkin BS (2009). The role of ongoing dendritic oscillations in single-neuron dynamics. *PLoS Comput Biol* **5**, e1000493.
- Remme MWH, Lengyel M & Gutkin BS (2010). Democracy-independence trade-off in oscillating dendrites and its implications for grid cells. *Neuron* **66**, 429–437.
- Remme MWH & Rinzel J (2011). Role of active dendritic conductances in subthreshold input integration. *J Comput Neurosci* **31**, 13–30.
- Roberts M, Lowet E, Brunet N, TerWal M, Tiesinga P, Fries P & DeWeerd P (2013). Robust Gamma Coherence between Macaque V1 and V2 by Dynamic Frequency Matching. *Neuron* **78**, 523–536.
- Scheffer-Teixeira R, Belchior H, Leao RN, Ribeiro S & Tort ABL (2013). On High-Frequency Field Oscillations (>100 Hz) and the Spectral Leakage of Spiking Activity. *J Neurosci* **33**, 1535–1539.
- Schomburg EW, Anastassiou Ca, Buzsáki G & Koch C (2012). The spiking component of oscillatory extracellular potentials in the rat hippocampus. *J Neurosci* **32**, 11798–811.
- Stuart G, Spruston N & Häusser M (2007). *Dendrites* Oxford University Press, Oxford, UK.
- Taxidis J, Anastassiou CA, Diba K, Koch Correspondence C & Koch C (2015). Local Field Potentials Encode Place Cell Ensemble Activation during Hippocampal Sharp Wave Ripples. *Neuron* **87**, 590–604.
- Tomsett RJ, Ainsworth M, Thiele A, Sanayei M, Chen X, Gieselmann MA, Whittington MA, Cunningham MO & Kaiser M (2015). Virtual electrode recording tool for extracellular potentials (vertex): comparing multi-electrode recordings from simulated and biological mammalian cortical tissue. *Brain Struct Funct* **220**, 2333–2353.

Williams SR & Stuart GJ (2000). Site independence of EPSP time course is mediated by dendritic I(h) in neocortical pyramidal neurons. *J Neurophysiol* **83**, 3177–3182.

Zhuchkova E, Remme MWH & Schreiber S (2013). Somatic versus dendritic resonance: differential filtering of inputs through non-uniform distributions of active conductances. *PloS One* **8**, e78908.

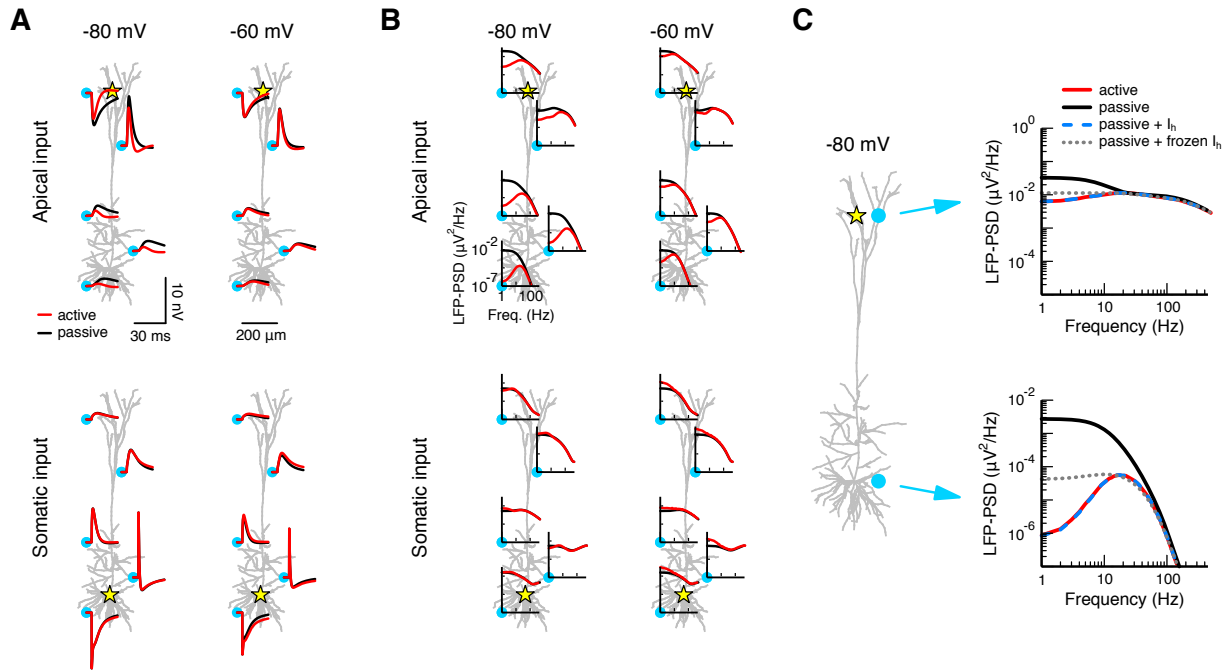


Figure 1: Active conductances can shape the extracellular signature of synaptic inputs. **A:** A single synaptic input is provided to a cortical layer 5 pyramidal cell model. The extracellular response is shown at five positions (cyan dots) for two cases: the active model that includes various voltage-dependent conductances (red; see Methods), or a passive model from which the active conductances have been removed (black). The position of the input is marked by the yellow star: at the distal apical dendrite (top panels) or at the soma (bottom panels). The cell's resting potential was held uniformly at a hyperpolarized potential of -80 mV (left panels) or at a depolarized potential of -60 mV (right panels). The synaptic peak conductance was 0.001 μ S. The plots show the x, z -plane of the cell; the soma and the electrodes are positioned at $y=0$. **B:** As in panel A, but using white-noise current input (see Method section) instead of synaptic input, and displaying the response as the power spectral density (PSD). The PSD is calculated from 1000 ms long simulations. **C:** Apical input (marked by star) to the cell model held at a hyperpolarized potential (-80 mV). The extracellular potential is shown at two positions (cyan dots) for the active (red) and passive (black) model and for two additional versions of the model: the passive model supplemented by I_h (dashed blue), and the passive model supplemented by frozen I_h (dotted gray; see Methods).

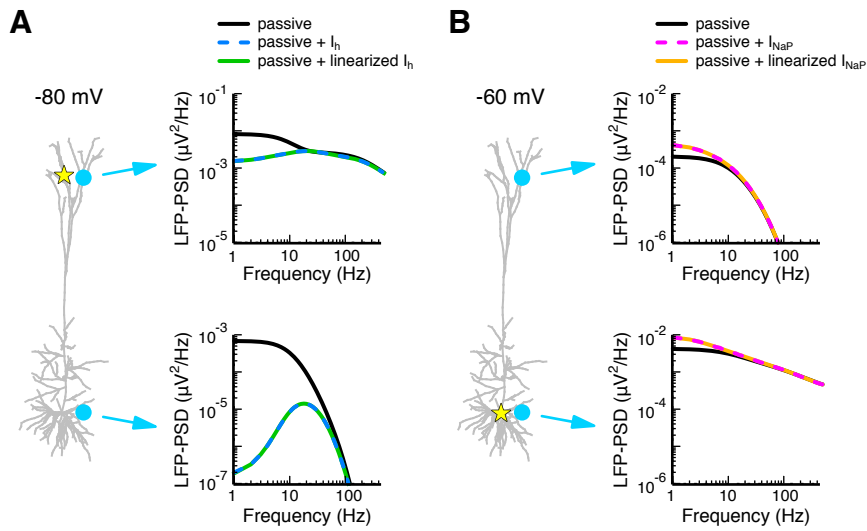


Figure 2: **Quasi-active conductances accurately mimic the responses of nonlinear conductances.** **A:** Apical white-noise current input (yellow star) is provided to a cortical pyramidal cell model held at a hyperpolarized potential (-80 mV). The LFP-PSD is shown at two locations (cyan dots) for a passive model (black), a passive model with I_h (dashed blue), and a passive model that includes a linearized or quasi-active I_h (green; see Methods). **B:** As in panel A, but with somatic white noise-current input and using the following three models: a passive model (black), a passive model with I_{NaP} (dashed magenta), and a passive model with linearized I_{NaP} (orange).

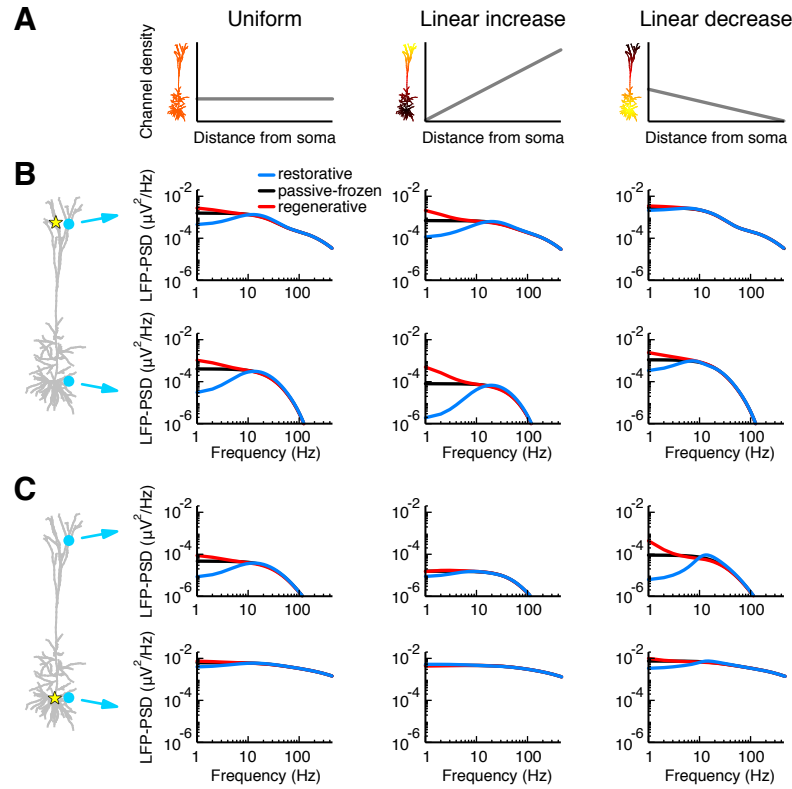


Figure 3: The type of active conductance, its distribution across the cell membrane, and the location of the input shape the LFP. **A:** A single quasi-active conductance was distributed across the pyramidal cell model in three ways: uniformly (left), linearly increasing (center), or linearly decreasing (right) with distance from the soma. The density of the linearly increasing conductance increased sixty-fold from the soma to the most distal apical dendrite, while the linearly decreasing conductance had a sixty-fold decrease over the same range. **B:** Apical white-noise current input (yellow star) was provided to the cell model and the LFP-PSD was determined at two positions (cyan dots). The quasi-conductance was either regenerative (red), passive-frozen (black) or restorative (blue). The three cases had the same total resting membrane conductance and the total passive leak conductance was equal to the total quasi-active conductance. **C:** As panel B, but with white-noise current input provided to the soma.

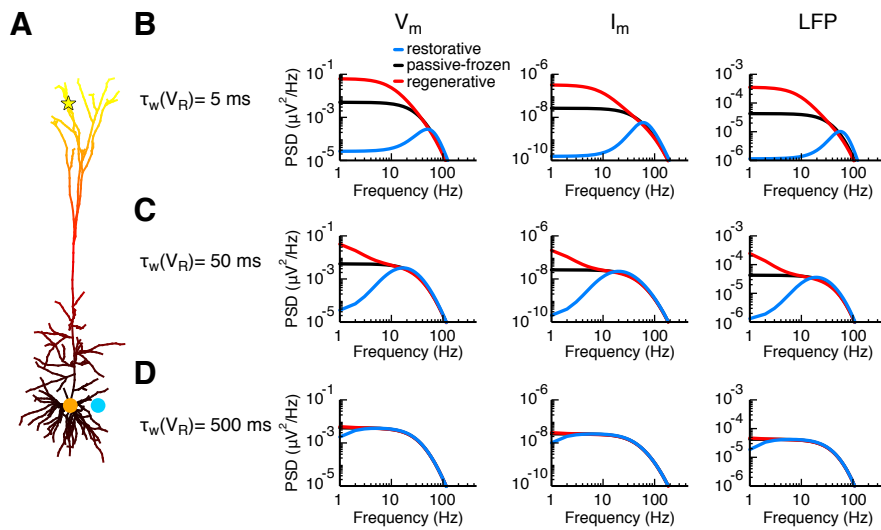


Figure 4: **Activation time constants of active conductances determine the frequencies for which they affect the LFP.** **A:** Apical white-noise current input (yellow star) to the cortical pyramidal cell model with a single linearly increasing quasi-active conductance (as in middle column of Fig. 3B). **B:** The quasi-active conductance is either restorative (blue), passive-frozen (black) or regenerative (red), and the PSD is shown for the somatic membrane potential V_m (left panel), the somatic transmembrane currents I_m (middle panel), and the LFP (right panel) at a position close to the soma (cyan dot). The activation time constant of the quasi-active conductance is $\tau_w(V_R) = 5$ ms. **C:** As panel B, but with $\tau_w(V_R) = 50$ ms. **D:** As panel B, but with $\tau_w(V_R) = 500$ ms.

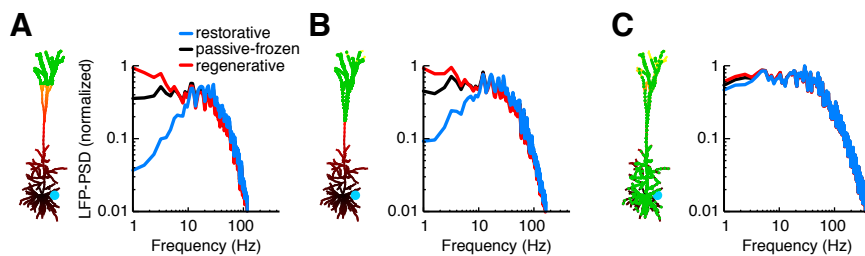


Figure 5: Resonance is retained for asymmetric input from distributed synapses. **A:** The pyramidal cell model expressed a single linearly increasing quasi-active conductance (see Figure 4A) that was either restorative (blue), passive-frozen (black), or regenerative (red). 1000 excitatory conductance-based synapses (green dots) with a peak conductance of $0.0001 \mu\text{S}$ were distributed across the distal apical tuft more than $900 \mu\text{m}$ away from soma. The synapses were activated by independent Poisson processes with a mean rate of 5 spikes per second. Simulations were run for 20 seconds and the LFP-PSD was calculated using Welch's method. **B:** As panel A, but with synapses distributed above the main bifurcation, $600 \mu\text{m}$ away from the soma. **C:** Synapses were distributed uniformly across the entire cell.

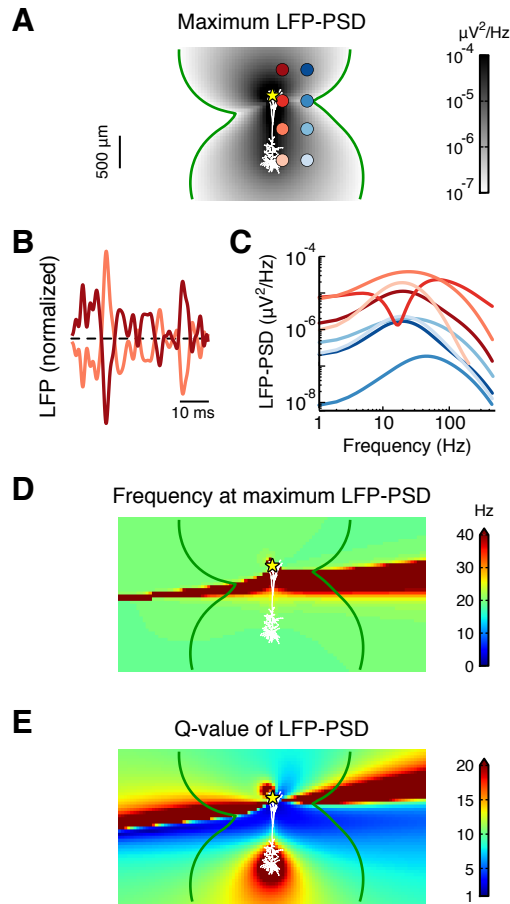


Figure 6: **Resonance in the LFP resulting from a restorative conductance is a spatially stable feature.** **A:** Apical white-noise current input (yellow star) is provided to the cortical pyramidal cell model with a single quasi-active conductance with increasing density with distance from soma. The resulting LFP-PSD was calculated at a dense 2D-grid surrounding the cell. The maximum power of the LFP is denoted in shades of gray. The green contour line shows where the LFP power is $10^{-7} \mu\text{V}^2/\text{Hz}$. **B:** Excerpts of LFP time traces at two extracellular positions, corresponding to the two electrodes at the opposite side of the zero crossing region of the dipole in panel A (i.e., the first and third electrode contact in the left column). **C:** LFP-PSD computed at the eight electrode positions marked by shades of red and blue in panel A. **D:** The frequency for which the LFP-PSD shows the maximum power (see panel A). **E:** The Q-value of the LFP-PSD, defined as the maximum power (see panel A) divided by the power at 1 Hz.

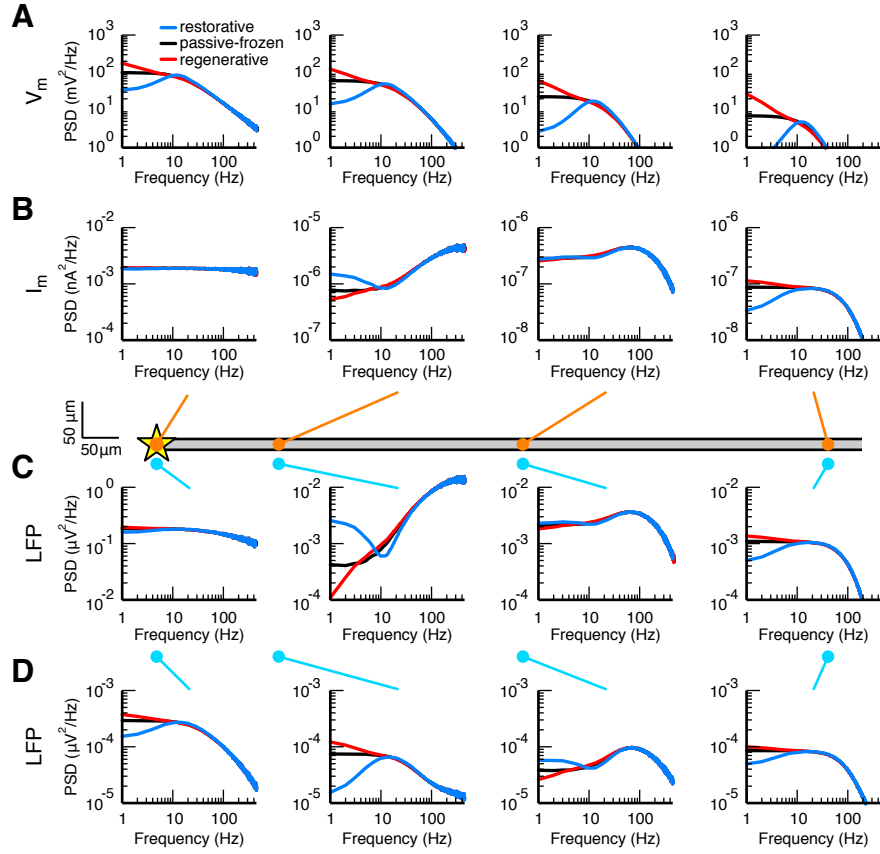


Figure 7: **Voltage, transmembrane current, and LFP for a semi-infinite neurite with a quasi-active conductance.** White-noise current input (yellow star in schematic above panel C) was applied to the end of a semi-infinite neurite with a single quasi-active conductance that was either restorative (blue), passive-frozen (black) or regenerative (red). The neurite had length 2000 μm , diameter 2 μm , intracellular resistivity $R_a = 100 \Omega \text{cm}$, and the passive leak and quasi-active conductance density were both uniformly set to 50 $\mu\text{S}/\text{cm}^2$. **A:** The membrane potential PSD (V_m) is shown at the positions marked by the orange dots in the schematic (at 0, 177, 531 and 973 μm distance from the input). **B:** As in panel A, but showing the transmembrane current PSD at the positions of the orange dots. **C:** As in panel A, but showing the LFP-PSD for the positions marked by the cyan dots (20 μm away from the neurite). **D:** As in panel C, but showing the LFP-PSD for electrodes at 300 μm away from the neurite, marked by the cyan dots.